variable	description	units
C_0	heat capacity of the surface skin layer	J m^{-2} K^{-1}
T_0	temperature of the surface skin layer	K
R_n	net radiation	W m^{-2}
H	sensible heat flux at the surface	W m^{-2}
G	ground heat flux (to ground, roof or wall)	W m^{-2}
θ_0	potential temperature at the surface	K
θ_1	potential temperature of the air grid adjacent to the surface	K
h	heat flux coefficient	W m^{-2} K^{-1}
$T_{matter,1}$	temperature of the outermost layer of the material	K
Λ	heat conductivity between the skin layer and the first grid level in the material	W m^{-2} K^{-1}
$F^d_{A \to B}$	differential view factor	m^{-2}
$\widehat{F}^d_{A \to B}$	normalized differential view factor	m^{-2}
$\mathcal{A}(B)$	surface area of face B	m^2
θ_A, θ_B	angles between face normals and the connecting ray	rad
s	length of ray	m
$J_{e,A \to B}$	irradiance of face B that comes from face A	
$E_{e,A}$	radiosity of face A	W m^{-2}
$SVF_{A \to B}$	irradiance factor	1 (dimensionless)
$RCSF_{C,A \to B}$	ray canopy sink factor of the ray $A \to B$ and the grid box C	1
a_C	leaf area density of grid box C	m^2 m^{-3}
s_C	length of the ray's intersection with box C	m
α	extinction coefficient	1
$T_{A \to B}$	total transmittance of the ray $A \to B$	1
Φ_e	radiant flux	W
$CSF_{C,A}$	ratio between the radiant flux absorbed within plant canopy box C originating from face A and the radiosity of face A	m^{-2}
$E_{e,dir}$	direct solar irradiance	W m^{-2}
$\mathcal{A}'_C$	cross-sectional area of C viewed from the direction of the solar radiation	m^{-2}
ε	surface emissivity	1

Table S1: Variables description

category	surface material	storage material	ε	Λ	roughness	roughness_h	C_0	thickness	ϱc	lambda_h
1	asphalt	asphalt concrete/gravel	0.93	41	0.002	0.002	14472	1	1360	1.6
2	pavement cobbles light	white granite/gravel/sand	0.93	54	0.003	0.003	16737	1	1360	1.6
3	paving blocks	concrete/gravel	0.93	66	0.003	0.003	22264	1	1360	1.6
4	pavement cobble	granite/gravel/soil	0.93	103	0.01	0.01	28629	1	1360	1.6
5	playground	plastic/sand	0.93	21	0.002	0.002	15972	1	1320	1.5
6	sand	sand	0.76	41	0.01	0.01	16571	1	1370	0.7
7	grass	soil	0.96	41	0.01	0.01	9075	1	1370	1.5
101	asphalt belt	softwood	0.93	69	0.001	0.001	3473	0.3	1144	0.3
102	sheet metal	softwood	0.93	69	0.001	0.001	4153	0.3	1144	0.3
103	concrete/fired tile	concrete/brick/wood	0.7	83	0.01	0.01	6353	0.35	1144	0.5
104	grass	soil	0.96	92	0.01	0.01	8168	0.45	1500	1
201	metal plate	brick	0.93	118	0.0002	0.0002	4235	0.35	1510	1
202	brick	brick	0.93	118	0.0012	0.0012	6395	0.35	1510	1
203	smooth brick	brick	0.93	118	0.001	0.001	6395	0.35	1510	1
204	smooth pavement	brick	0.93	83	0.0003	0.0003	7454	0.35	1510	1
205	smooth cobblestone	brick	0.93	59	0.0007	0.0007	7454	0.35	1510	1
206	plaster	brick	0.93	83	0.0009	0.0009	7454	0.35	1510	1
207	plaster	burnt breeze block	0.93	83	0.0009	0.0009	6776	0.35	1000	0.7
208	plaster + bricks	brick	0.93	118	0.001	0.001	6564	0.35	1510	1
209	plaster + vegetation	brick	0.95	118	0.005	0.005	6564	0.35	1510	1
210	plaster + tiling	brick	0.93	118	0.001	0.001	7411	0.35	1510	1
211	plaster + glass	brick	0.93	83	0.0007	0.0007	8894	0.35	1510	1
212	plastic	brick	0.93	83	0.0007	0.0007	8470	0.35	1510	1
213	glass	brick	0.92	118	0.0007	0.0007	5506	0.35	1510	1
214	glass	insulation	0.92	118	0.0007	0.0007	4235	0.35	1000	0.5
215	plaster + glass	burnt breeze block	0.92	138	0.0007	0.0007	3630	0.3	1000	0.5
216	plaster + glass	insulation	0.93	138	0.0008	0.0008	8894	0.3	1000	0.5
217	decorated plaster	brick	0.93	118	0.0011	0.0011	7454	0.35	1510	1

Table S2: ε ... emissivity, Λ ... heat conductivity of the surface skin layer (W m^{-2} K^{-1}), *roughness* applies to momentum variables while *roughness_h* applies to scalar variables, C_0 ... surface skin layer heat capacity (J m^{-2} K^{-1}), thickness ... (m), ϱc ... volumetric heat capacity of the material (kJ m^{-3} K^{-1}), *lambda_h* ... thermal conductivity (W m^{-1} K^{-1})

location / point	height (m)	category	albedo
Loc. 1 / point 1	13.3	207	0.4
Loc. 1 / point 2	5.6	207	0.4
Loc. 1 / point 3	13.4	206	0.3
Loc. 1 / point 4	13.4	206	0.3
Loc. 1 / point 5	8.4	206	0.3
Loc. 1 / point 6	4	206	0.4
Loc. 2 / point 1	4.3	217	0.5
Loc. 2 / point 2	1.1	203	0.5
Loc. 2 / point 3	6.2	217	0.5
Loc. 2 / point 4	8.6	217	0.5
Loc. 2 / point 5	1.1	203	0.5
Loc. 3 / point 1	8.9	206	0.2
Loc. 3 / point 2	5.2	206	0.2
Loc. 3 / point 3	9	206	0.2
Loc. 3 / point 4	1.4	206	0.7
Loc. 4 / point 1	3.3	206	0.4
Loc. 4 / point 2	6.1	206	0.2
Loc. 4 / point 3	14.5	206	0.2
Loc. 4 / point 4	14.6	216	0.6
Loc. 4 / point 5	14.6	216	0.6
Loc. 4 / point 6	3.6	214	0.6
Loc. 4 / point 7	1.8	214	0.6
Loc. 5 / point 1	2.5	207	0.7
Loc. 5 / point 2	5.9	207	0.15
Loc. 5 / point 3	13.2	207	0.15
Loc. 5 / point 4	2.2	203	0.35
Loc. 5 / point 5	13.4	206	0.35
Loc. 6 / point 1	2.3	207	0.15
Loc. 6 / point 2	5.9	207	0.15
Loc. 6 / point 3	7.9	207	0.15
Loc. 6 / point 4	2.3	217	0.65
Loc. 6 / point 5	6	217	0.3
Loc. 6 / point 6	8.7	217	0.3
Loc. 7 / point 1	2.4	217	0.55
Loc. 7 / point 2	6.6	217	0.55
Loc. 7 / point 3	9.8	217	0.55
Loc. 8 / point 1	0	2	0.4
Loc. 8 / point 2	0	1	0.1
Loc. 8 / point 3	0	1	0.3
Loc. 8 / point 4	0	1	0.1
Loc. 8 / point 5	0	4	0.3
Loc. 8 / point 6	0	4	0.3
Loc. 8 / point 7	0	4	0.3
Loc. 8 / point 8	0	4	0.3
Loc. 9 / point 1	4	206	0.45
Loc. 9 / point 2	7.4	206	0.45
Loc. 9 / point 3	9.9	206	0.45
Loc. 9 / point 4	1	206	0.4
Loc. 9 / point 5	4	206	0.4

Table S3: Parameters of evaluation points
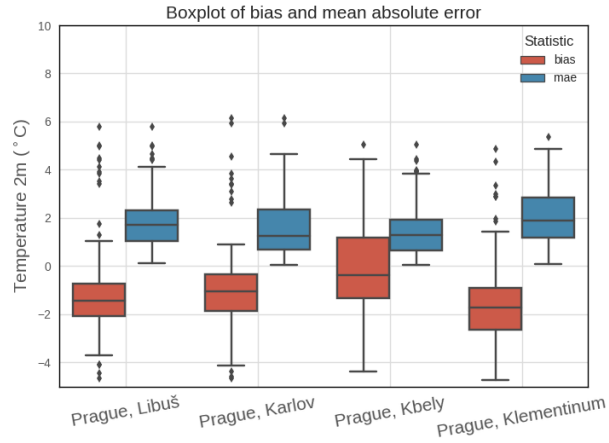
Figure S1: Bias and mean absolute error of the WRF model (hourly data) for the period of 1–5 July 2015.
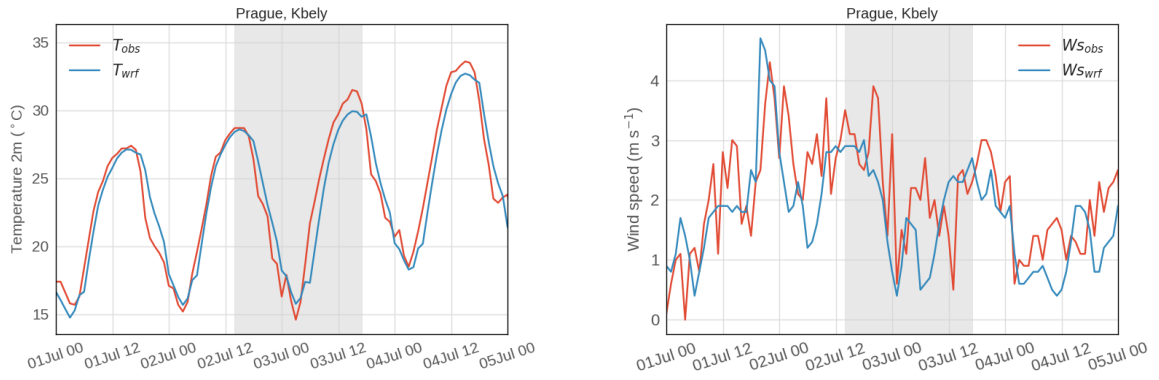

Figure S2: Comparison of WRF time series of temperature (left) and wind speed (right) to values measured at Prague, Kbely station. Shaded areas mark the time of the observation campaign.
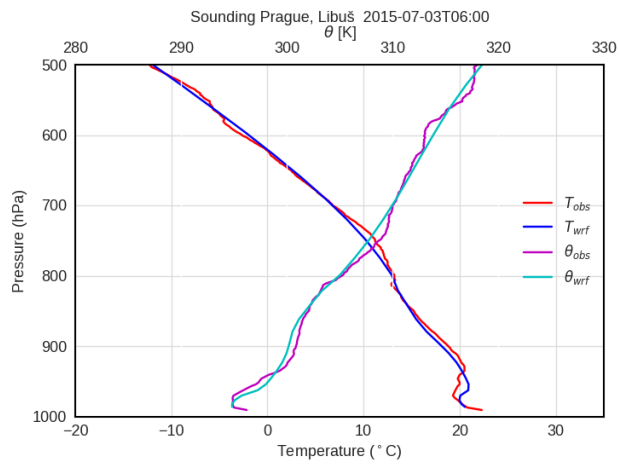

Figure S3: Comparison of WRF vertical profiles of absolute temperature (T) and potential temperature (θ) to values measured at Prague, Libuš station on 3 July 06:00 UTC.
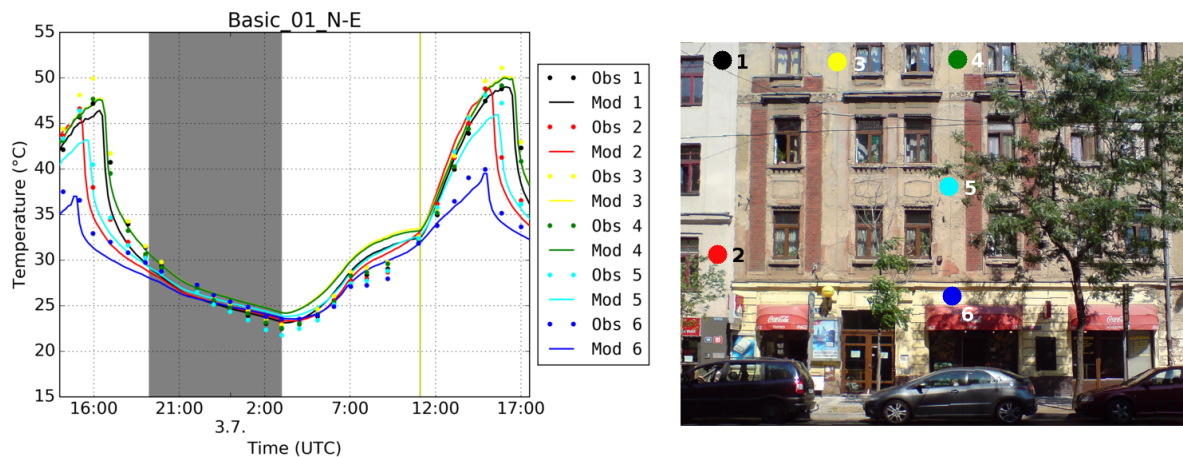
Figure S4: Comparison of modelled and observed surface temperatures from the observation location 1 (50.10344N, 14.44983E) – view of west facing wall. The graph shows comparisons for chosen evaluation points for the period of observation campaign from 2 July 2015, 14:00 UTC to 3 July 2015, 17:00 UTC. The solid line represents modelled values while the dots show the observed values. The shaded area depicts nighttime and yellow vertical line depicts solar noon.
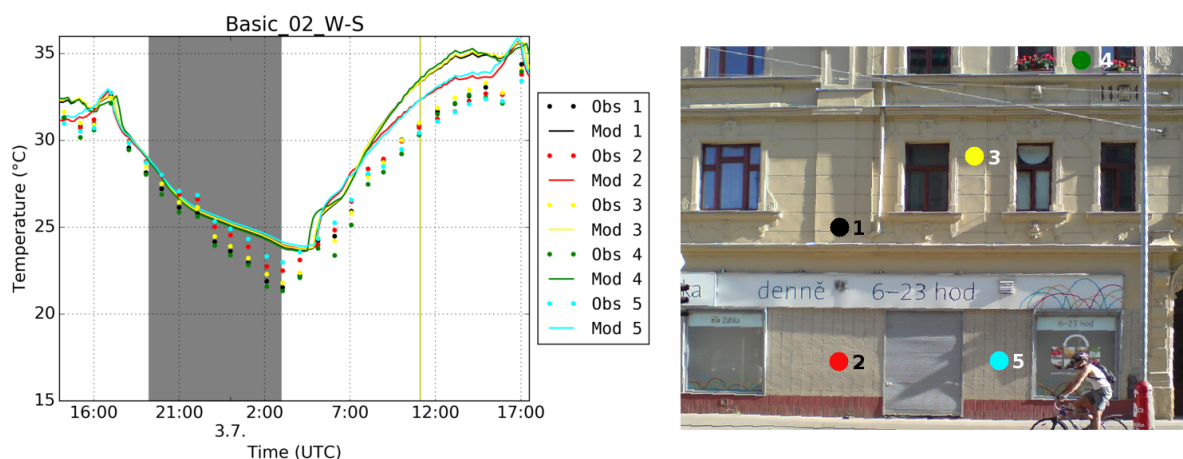
Figure S5: As Fig. S4 for location 2 (50.10327N, 14.44963E) — view of north facing wall.
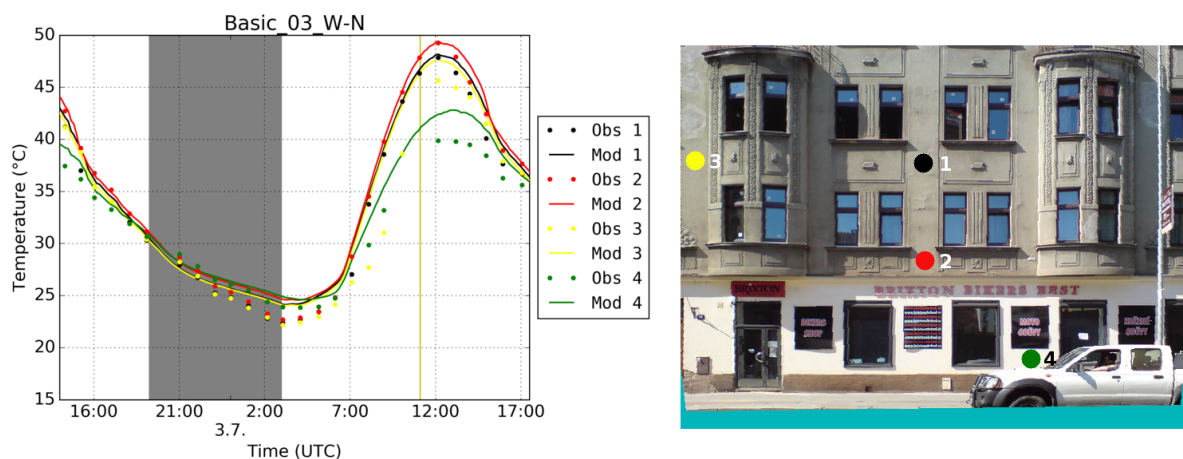
Figure S6: As Fig. S4 for location 3 (50.10317N, 14.44932E) — view of south facing wall.
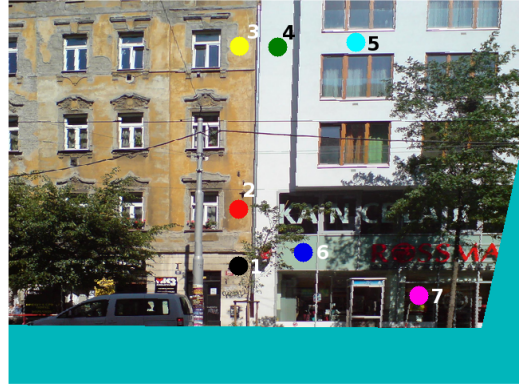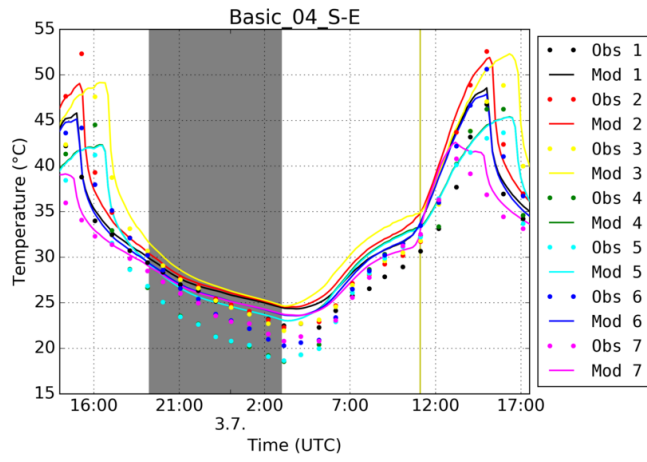
Figure S7: As Fig. S4 for location 4 (50.10288N, 14.44985E) — view of west facing wall.
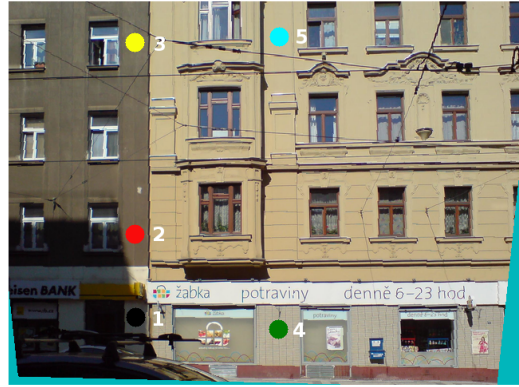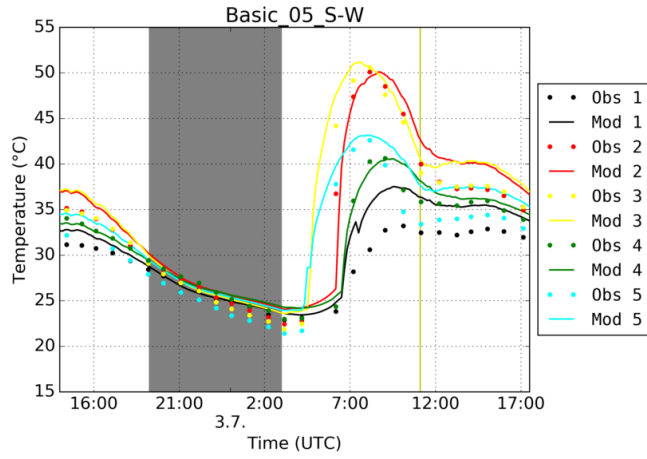
Figure S8: As Fig. S4 for location 5 (50.10300N, 14.45010E) — view of east facing wall.
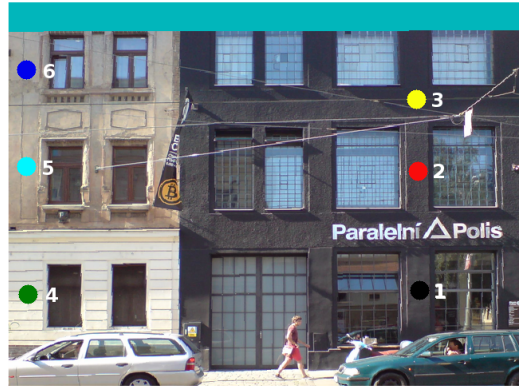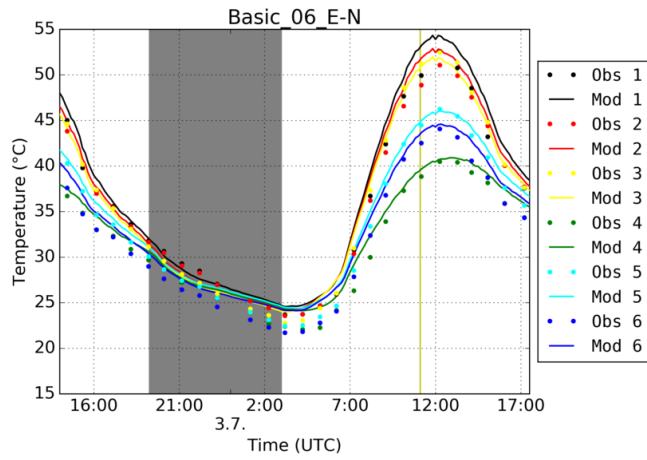
Figure S9: As Fig. S4 for location 6 (50.10318N, 14.45042E) — view of south facing wall.
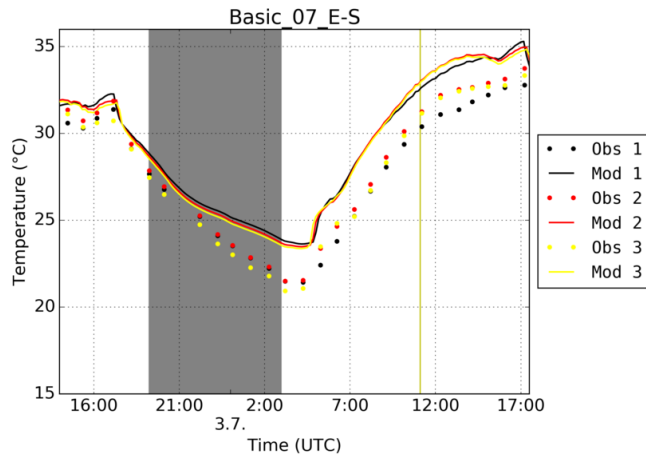
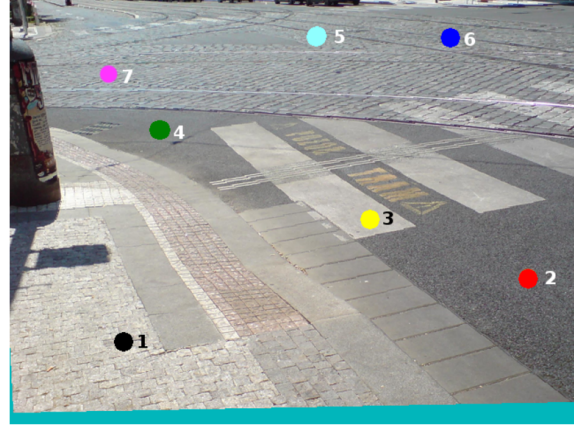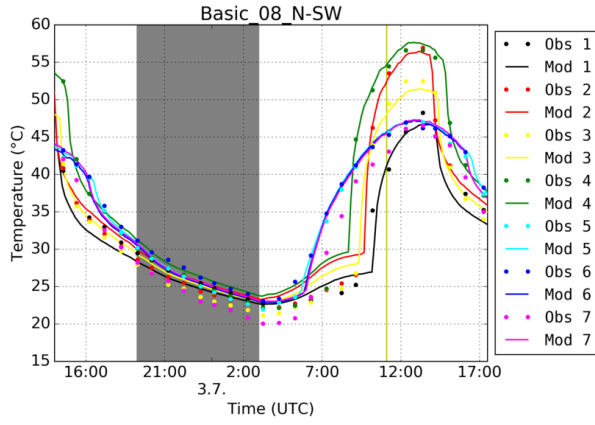Figure S10: As Fig. S4 for location 7 (50.10329N, 14.45040E) — view of north facing wall.

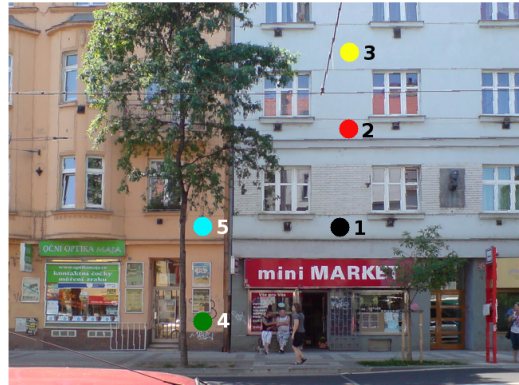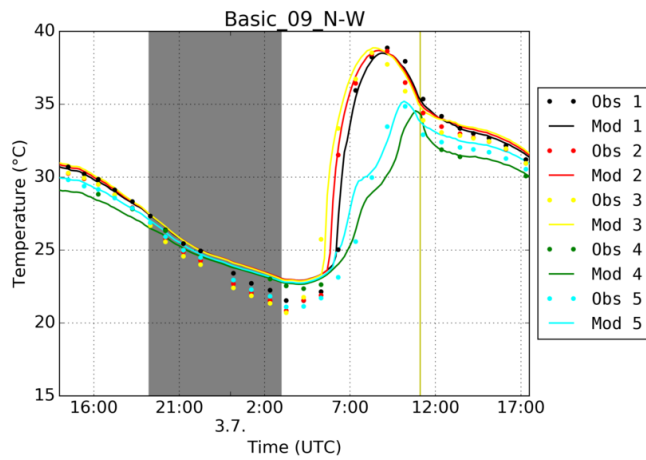Figure S11: As Fig. S4 for location 8 (50.10340N, 14.45007E) — view of ground on the crossroads.

Figure S12: As Fig. S4 for location 9 (50.10354N, 14.45006E) — view of east facing wall.

Figure S13: Infrared snapshot from observation location 3 (50.10354N, 14.45006E) — view of south facing wall from 3 July 2015 08:05 UTC (10:05 local time).
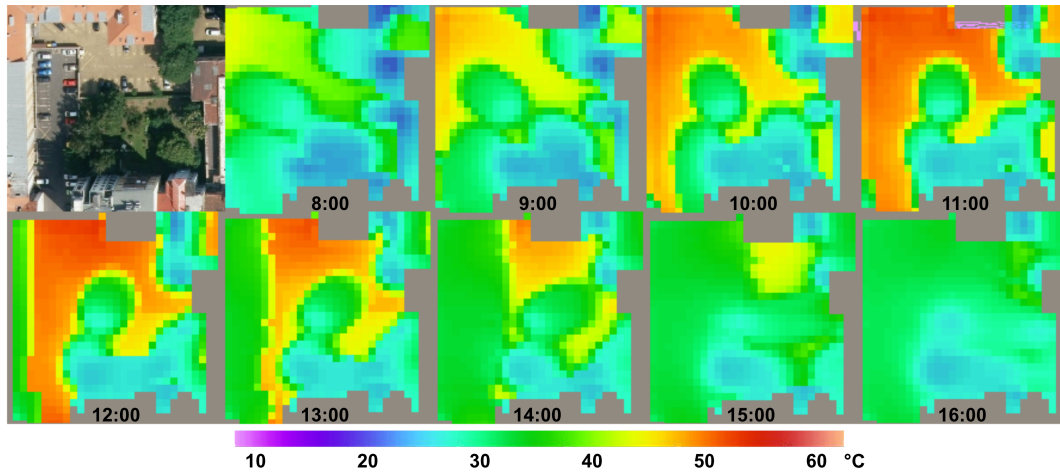

Figure S14: Aerial photo and modelled surface temperature of the pavement in the courtyard in the south-west corner of the domain (50.10368N, 14.44759E) for hours from 08:00 UTC to 16:00 UTC on 3 July.

Figure S15: Three infrared snapshots from observation location 6 — view of south facing wall from 3 July 2015 01:08 UTC (03:08 local time), 10:08 UTC (12:08 local time) and 13:17 UTC (15:17 local time).